Thickness dependence of poly(tryaryl amine) hole transport layer on bulk heterojunction organic solar cells

K. L. USHA KUMARY[a], M. PRATHEEK[b], T. A. SHAHUL HAMEED[c], P. PREDEEP[b,*]
[a]*LBS Centre for Science and Technology, Trivandrum, 695033, India*
[b]*Laboratory for Molecular Electronics and Photonics, National Institute of Technology, Calicut, 673601, India*
[c]*Department of Electronics and Communication Engineering, TKM College of Engineering, Kollam, 691005, India*

Transport layers have a critical role in the performance of bulk heterojunction (BHJ) solar cells. In this work, poly(tryaryl amine) (PTAA) was introduced as the hole transport layer (HTL) in the device with the structure ITO/PTAA/P3HT:PCBM/Al. The electrical carrier transport properties of the devices were studied with PTAA layer in varying thicknesses and spin speed. It has been observed that the PTAA which was coated at a spinning speed of 2000rpm exhibited better performance compared to those spin cast at higher speeds. Impedance measurements with an ac voltage of 10mV amplitude at different bias voltages, were carried and the effect of capacitance, resistance and conductance for a range of frequencies investigated, which is expected to shed light on the possibilities of incorporating more versatile layers in such devices.

(Received June 29, 2020; accepted June 11, 2021)

Keywords: Carrier concentration, PTAA, Rectification

1. Introduction

The research in organic photovoltaics has gained momentum for more than a decade due to its lightweight, low-temperature processing and flexiblity. The bulk heterojunction (BHJ) organic photovoltaic (OPV) cells prepared by a composite of donor and acceptor organic semiconductors have more significance owing to their greater conversion efficiency. The major processes in an OPV are excitons generation, diffusion of excitons to the donor/acceptor interfaces, dissociation of excitons into charge carriers and finally a collection of charge carriers by the electrodes. Due to the efficient excitons dissociation and higher carrier mobility, P3HT:PCBM BHJ is widely used [1] in OPV devices. The nature of the interfaces between the active layer and electrodes is very important in the overall performance and lifetime of the OPVs and it is required to have a good ohmic contact at the interface. Interfacial materials play a vital role in improving the lifetime and efficiency of OPVs and the selection of such materials carry significance with respect to the matching of work functions with the energy levels of donors and acceptors in the device. This in turn improves charge selectivity of the electrodes and modifies surface morphologies [2-4] of the active materials. Studies [5-6] reveal that BHJ morphologies can be improved by different techniques which enhance the photovoltaic performance.

The organic semiconductor, poly(triaryl amine) PTAA is a stable and solution-processable polymer with hole mobility that varies from 10^{-3} to $10^{-2}cm^2/VS$. The effect of PTAA on the OPV depends on the solvent type and concentration, spinning speed, annealing temperature and the duration in which annealing is carried out [7].

In this article, PTAA was introduced as the hole transport layer (HTL) in the BHJ OPV device in which P3HT and PCBM combination forms the active layer. The influence of PTAA with varying thicknesses on the device performance was investigated. The thin layer of PTAA was prepared by spin coating which produces uniform layers. The layer was evenly coated onto the substrate at higher spinning speed due to the centripetal force together with the surface tension of the solution. The high-speed spinning causes the solvent evaporation which leaves the material on the surface and the film obtained after the spin coating has a thickness that is proportional to the spinning speed as $t \alpha 1/\omega^{1/2}$ where t and ω are the film thickness and spin speed. The devices were fabricated with the PTAA layer coated onto the ITO substrate at different spinning speeds to obtain the layers with varying thicknesses. It is understood that [8] the photovoltaic properties vary with the thickness of HTL as it varies with the resistance and work function of the layer.

2. Experimental

Fig. 1 shows materials molecular structure, energy levels and device configuration ITO/PTAA/P3HT:PCBM/Al [9-11].

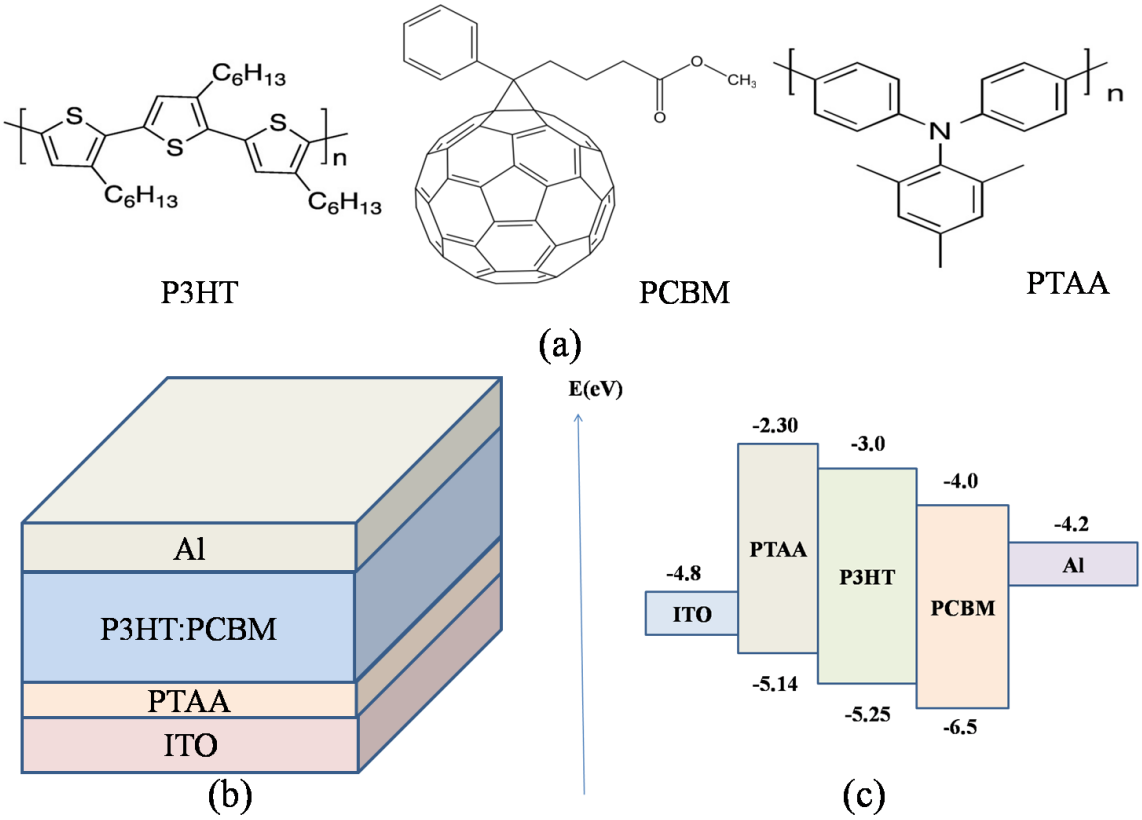

Fig. 1. (a) Structures of P3HT, PCBM and PTAA (b) OPV device (c) Energy band diagram (color online)

The materials P3HT, PCBM and PTAA purchased from Sigma-Aldrich were directly used for fabricating the device. The ITO coated glass substrates (76Ω/cm^2) were initially cleaned by sonicating in 0.1% Hellmanex solution and further in isopropyl alcohol and also by UV ozone cleaner [12-13]. The 0.2% PTAA solution was prepared in toluene and stirred for 1hr in a glove box. It was spin-coated onto the ITO glass substrate at different spinning speeds 2000 rpm, 3000 rpm and 4000 rpm. P3HT and PCBM were intermixed in equal proportion in 1,2-dichlorobenzene and stirred for 12hrs at 70 ^{o}C. The blend was coated onto the PTAA layer at a spinning speed of 1000 rpm for 65s. Al (cathode) was evaporated to get a layer thickness of 106 nm.

A Keithley Source Meter in unison with a solar simulator at 100 mW/cm^2 was used to obtain the electrical characterizations of the devices made with different HTL thicknesses. Impedance measurement was carried out by Wayne Kerr 6500B Precision Impedance Analyser.

3. Results and discussions

OPV devices, device A, device B and device C were constructed in the same configuration ITO/PTAA/P3HT:PCBM/Al where the PTAA layer was coated with different spinning speeds of 2000 rpm, 3000 rpm and 4000 rpm respectively.

3.1. Dark current-voltage characteristics

The characteristics shown in Fig. 2 gives nonlinear and asymmetric characteristics that mimic a rectifier diode which is emerged from the presence of the Schottky barrier in the diode and it is due to [14-15] the effect of density of interface states, series resistance and the ideality factor.

The rectifying nature, reverse saturation current, the density of states and series/shunt resistances of the diode can be better explained from the semilogarithmic plot (Fig. 2(b)). The rectification behavior deduced from the voltage drop across the series resistance corresponds to a linear variation for the lower voltages and the linearity is seen here as not holding good for higher voltages. The ratio of the forward current to the reverse current by keeping the voltage constant better analyses this fact and the ratio obtained for device A, device B and device C at +/- 1V are 2.99×10^3, 8.9×10^1 and 8.5×10^2 respectively. It is found that even the ratios are not as high as to show better rectification behaviour, the device fabricated with HTL coated with 2000 rpm with better efficiency posses the highest rectification ratio. It implies that in device A, charge injection is higher during the forward bias and less in the reverse bias. It is also to be noted that the devices with PTAA coated with different spinning speeds have different thicknesses and morphologies and these may also have an effect on the diode properties [16]. The

barrier heights of electrons and holes usually decide the rectification ratio. In a homojunction diode, the barrier height seen by electrons and holes are the same and is equal to the barrier potential and at the same time, it is different in the heterojunction devices [17].

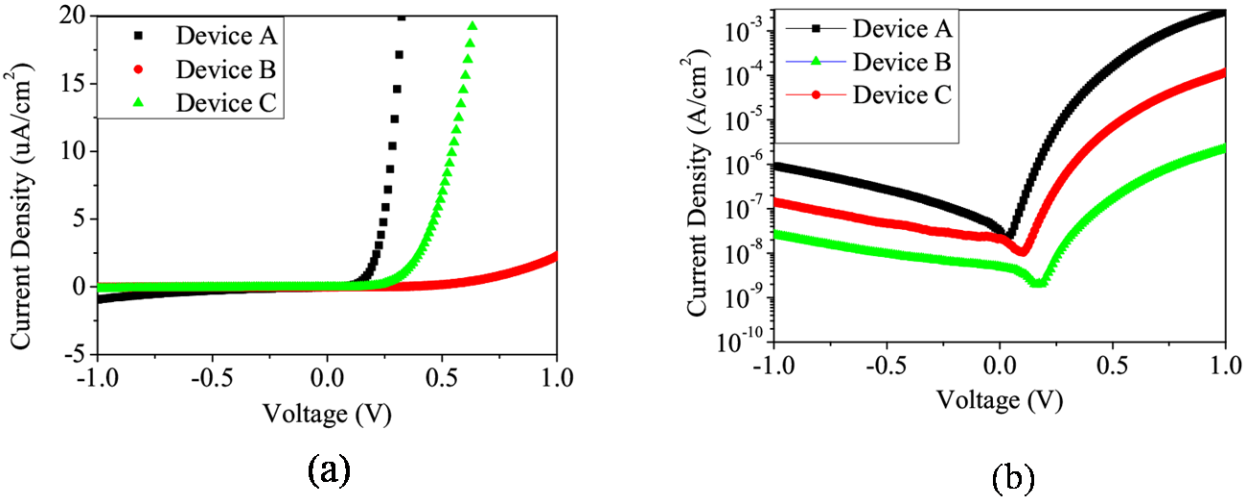

Fig. 2. Forward and reverse bias (a) J-V and (b)semi-logarithmic J-V dark characteristics (color online)

The characteristics in the semilogarithmic scale shown in Fig. 2(b) exhibits a linear variation at lower bias voltages and a downward curve at higher voltages, and this is attributed to the presence of the series resistance and interfacial states at the interface of metal/semiconductor. Shunt resistance R_{sh} is associated with the polymer-semiconductor and series resistance R_s is with the metal-semiconductor interfaces and so for the ideal diode, $R_s \approx 0$ and R_{sh} is of very high, in the order of megohms (MΩ) [14]. The values of R_{sh} and R_s obtained for the devices A, B and C were 2.37MΩ, 2.21MΩ and 2.17MΩ and 1MΩ, 1.44MΩ and 1.6MΩ respectively. The values show that R_{sh} reduces and R_s increases as thickness get reduced. Thus, it can be concluded that HTL coated at 2000rpm behaves better compared with other devices.

Barrier height at the zero bias and the reverse saturation current are related as [18]:

$$\phi_B = \frac{KT}{q}\ln(ART^2/I_o) \qquad (1)$$

where k-Boltzmann's constant, T-temperature in Kelvin, q- electron charge, A- the contact area of the rectifier, R-Richardson constant and Io is the reverse saturation current. Io can be obtained from the semilog J-V characteristics by taking the intercept of the straight line at V=0.

The values of Io determined for the devices are found to reduce from 3.24×10^{-8}mA/cm^2 to 4.73×10^{-9}mA/cm^2 and that of ϕ_B increases from 1.02eV to 1.09eV (with R=120 Acm^{-2}K^{-2}) [19] for the devices from device A to device C. The obtained value of ϕ_B may be at par with the optical band gap of P3HT:PCBM [20].

The carrier mobility of the devices based on different PTAA layers are estimated using the space charge limited current (SCLC) method and are found to be 0.4654×10^{-5}cm^2/VS and 0.1876×10^{-6}cm^2/VS for device A (2000 rpm) and device C(4000 rpm) respectively. It is understood that the mobility get reduced due to the lower electrical conductivity [21] of the PTAA layer when it becomes thinner.

3.2. Device Characteristics under illumination

The current-voltage characteristics of the devices are plotted in Fig 3.

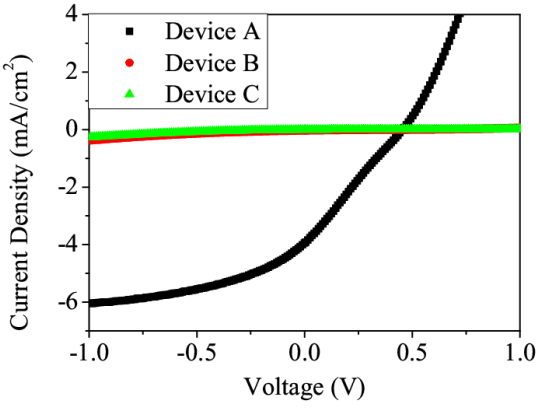

Fig. 3. J-V characteristics (color online)

Different parameters of OPV devices that is, short circuit current density (J_{sc}), open-circuit voltage (V_{oc}), fill factor and the power conversion efficiency (PCE) thus obtained are listed in Table 1 below:

Table 1. Parameters computed with different thicknesses of PTAA under the illumination of 100mW/cm^2

Device	Spinning Speed (rpm)	J_{sc} (mA/cm^2)	V_{oc} (V)	Fill Factor (%)	PCE (%)	R_s (Kohms)	R_{sh} (Kohms)
A	2000	3.940	0.462	24.18	0.440	0.138	0.161
B	3000	0.025	0.393	16.76	0.002	31.10	8.57
C	4000	0.00002	0.383	18.55	0.0001	31.20	24.90

As can be seen, the PV cell parameters vary significantly with the devices except in the case of V_{oc} and it is found that the variation of V_{oc} is not much compared to other parameters. The higher the spinning speed, the faster is the drying time which provides better consistency, but the poor performance of thinner PTAA layers may be attributed to the lack of time needed to self-assemble and/or crystallize the layer. The device with the highest thickness gives better efficiency due to the increase of short circuit current density and fill factor. The improved performance is due to the hole selective interface and ohmic contact at the anode which provided a better way to extract the holes and their transport to the electrode [22].

It can be further seen from Table 1 that device A which shows the highest efficiency has a smaller value of R_s compared to R_{sh}. It is known that the fill factor decreases when the series resistance increases at the PTAA/anode interface and the shunt resistance decreases. The layers coated with 3000 and 4000 rpms, the values of shunt resistances are lower than that of series resistances and it could be due to the surface inhomogeneities at the PTAA layer [15].

It is observed that the photovoltaic performance of the OPV device with the PTAA interface layer is not appreciable though better parameters are obtained with device A. The overall low performance may be due to the fabrication processes being carried out under the normal atmospheric conditions in which the humidity ranges from 60 to 75%. Further, the PTAA is inherently hydrophobic in nature. The contact angle of water measured for PTAA is about 85^0 (Fig. 4) and it is much larger compared to the wetting angle of PEDOT:PSS (25^0) which shows that the surface energy of PTAA is less than that of PEDOT:PSS. The hydrophobicity of PTAA affects the morphology and incomplete coverage of the active layer. This argument may little bit odd considering the fact that the P3HT/PCBM active layer is also hydrophobic. However, in the P3HT:PCBM bulk heterojunction, P3HT has been shown [23] to be relatively hydrophobic and PCBM relatively hydrophilic. Because of the different surface tension properties of these materials, it is known that PCBM tends to be at the bottom side (near to PTAA), once the bulk heterojunction is coated over it and this makes the interface more hydrophobic-hydrophilic than hydrophobic-hydrophobic. This must be the reason for the poor film morphology of the absorber on PTAA even though the blend contains a strong hydrophobic component P3HT and this can be the plausible reason for the poor interface compatibility and bad contact morphology the absorber layer suffers on the top of the hole transport layer, PTAA in the device studied here. This must he contributing to the overall poor efficiency of the device. The wettability issue may be alleviated through annealing assisted interdiffusion method, surfactant addition engineering and sophisticated pre-wetting methods. However, PTAA has substantial advantages over PEDOT:PSS like not hygroscopic as the latter. This advantage may result in more environmental stability for PTAA based device.

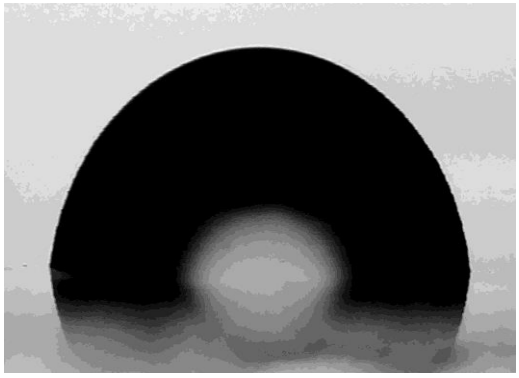

Fig. 4. Water contact angle on ITO/PTAA

3.3. Impedance Spectroscopy Analysis

The frequency-dependent capacitances of the devices are shown in Fig. 5. The capacitance has significant variation when the biasing voltage is more positive. The capacitance value is greater when the thickness is optimum in its performance and it reaches a steady value at higher frequencies due to the absence of charges flow through the device. The geometric capacitance, C_{geo} values obtained for the devices A and C are 106pF and 172pF respectively. At intermediate frequencies, C_{geo} reduces due to the injected carriers and at lower frequencies, the capacitance increases as there is an extra capacitance due to the trapping and release of charges from the traps in the material [24].

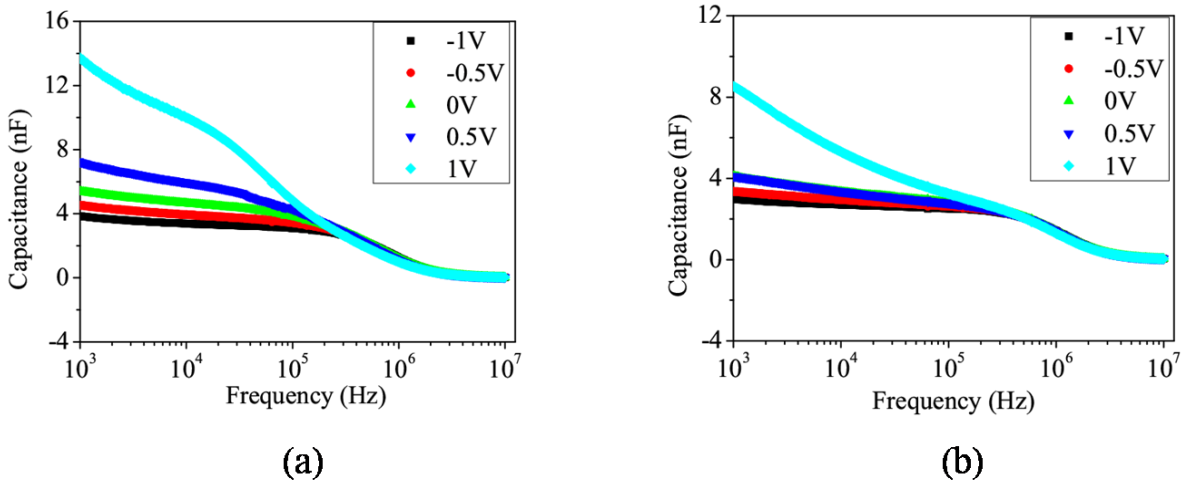

Fig. 5. Capacitance-frequency plot (a) Device A(2000 rpm) (b) Device C(4000 rpm) (color online)

The conductance variation with frequencies of the same device with varying bias voltages is given in Fig. 6. It is clear that conductance increases with biasing voltages as the injected holes are increased [25] and it has lower values with Device C.

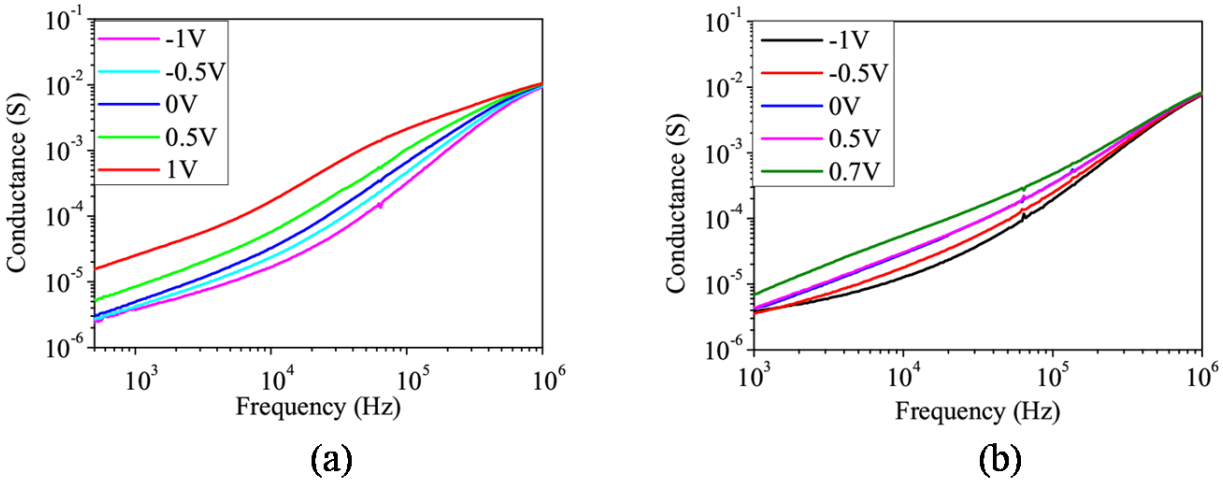

Fig. 6. Frequency dependent conductance (a) Device A(2000 rpm) (b) Device C(4000 rpm) (color online)

The resistance-frequency plot of the devices is shown in Fig. 7 for different biasing voltages.

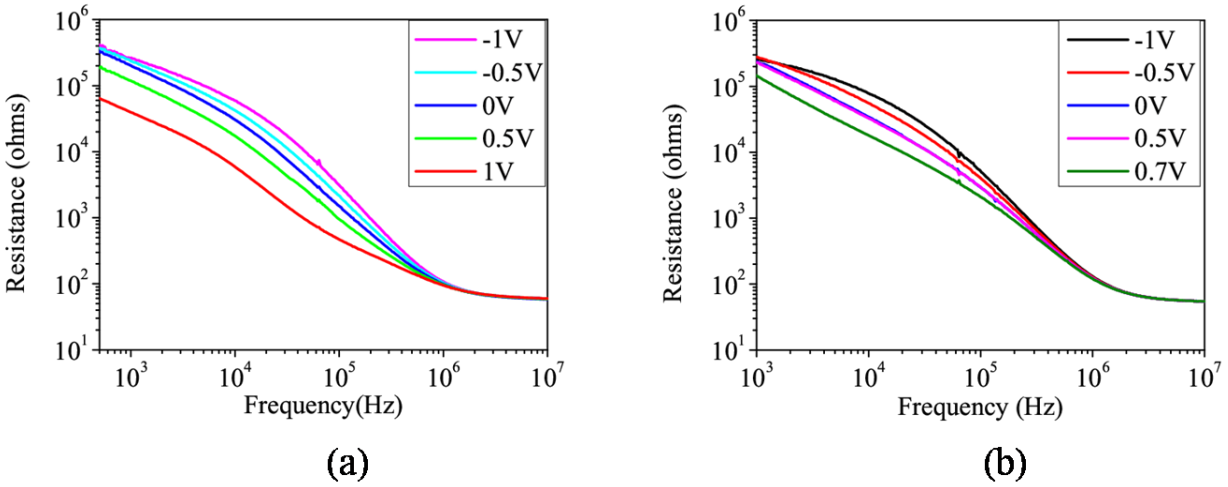

Fig. 7. Resistance-frequency variation (a) Device A(2000 rpm) (b) Device C(4000 rpm) (color online)

The hole mobilities can be computed from the negative differential susceptance (-ΔB) versus frequency plots in Fig. 8 using the measured capacitance C and the device capacitance C_{geo} as $-\Delta B = 2\pi f(C-C_{geo})$. The peak point of -ΔB corresponds to the frequency $f_r = \tau_r^{-1}$. With the bias voltage V and the device thickness d, using the expression $\mu=\frac{d^2}{\tau_{dc} V}$ where $\tau_{dc} = 0.56\tau_r$ [24], carrier mobility can be calculated.

The measurement of capacitance depends upon the space charge region present in a pn or Schottky junction and it varies inversely with its width. The space charge region width in turn depends upon the applied voltage V and also the doping concentration N_a. The variation of capacitance with the bias voltage, according to the Mott-Schottky relation [26] is given by,

$$C^{-2} = \frac{2(V_{bi}-V)}{A^2\varepsilon_0\varepsilon_r q N_a} \quad (2)$$

where V_{bi} is the built-in potential, ε_o- absolute permittivity, ε_r - permittivity of the organic semiconductor which is taken as 4 [27], A is the surface area of the device and q is the electron charge.

The capacitance-voltage characteristics of devices A and C are given in Fig. 9. The linearity is exhibited due to the formation of the Schottky junction between the metal and semiconductor.

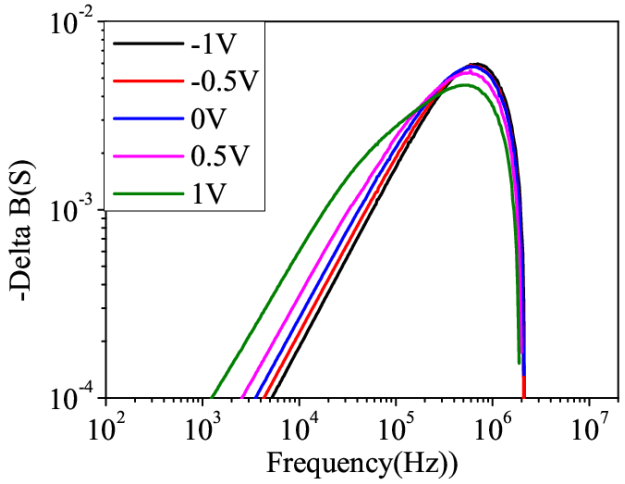

Fig. 8. Negative Differential Susceptance -ΔB obtained from the capacitance data (color online)

At uniform doping, N_a is constant and C^{-2}-V plot is a straight line. Its slope gives N_a and the intercept with the horizontal axis corresponds to the value of barrier potential at zero bias. From Fig. 9, the doping concentration N_a is obtained for device A is $1.1\times10^{17}/cm^3$ and $1.9\times10^{16}/cm^3$ for device C. These values indicate a reduced carrier concentration for device C. The depletion region of device A varies between 31.9 nm to 83.8 nm which is compatible with device thickness of 110 nm for the average potential applied between -1 and 1V [26].

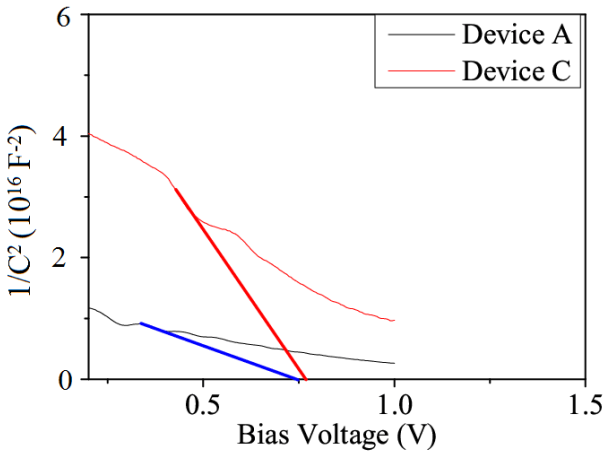

Fig. 9. C-V characteristics (color online)

The commonly used electrical equivalent of a solar cell (Fig. 10) in which the resistive losses in the electrodes and transport layers are represented by the series resistance R_s and active layer response by the combination of R_p and C_p. The equivalent circuit can be modelled accurately by the series combination of R_s and C_p or a parallel combination of R_p and C_p depending on the region in which the capacitance, resistance, frequency etc. dominates [28].

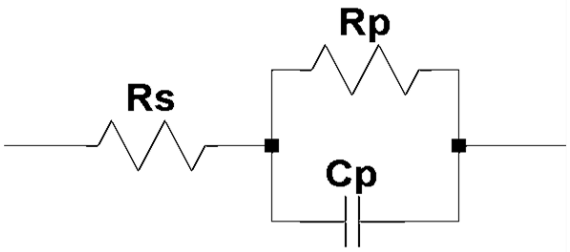

Fig. 10. Equivalent circuit

Fig. 11 shows the variation of impedance magnitude with the frequency of the devices A and C and from the impedance magnitude, the approximation, series/parallel can be selected. The boundary at which the approximation model changes is device-dependent. The smaller capacitance, as well as series resistances, may shift the parallel to series transition at higher frequencies. The general guidelines used are i) |Z| >10KΩ for parallel approximation, ii) |Z| <1KΩ for series approximation and iii) any of the above for 1K<|Z|<100KΩ [13].

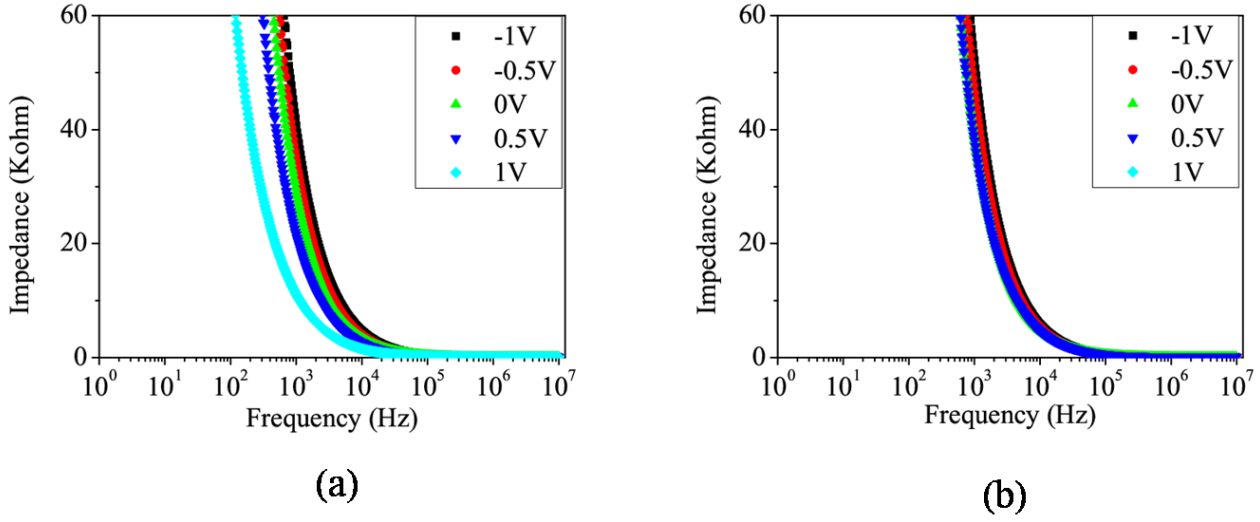

Fig. 11. Impedance vs frequency plot (a) Device A(2000 rpm) (b)Device C(4000 rpm) (color online)

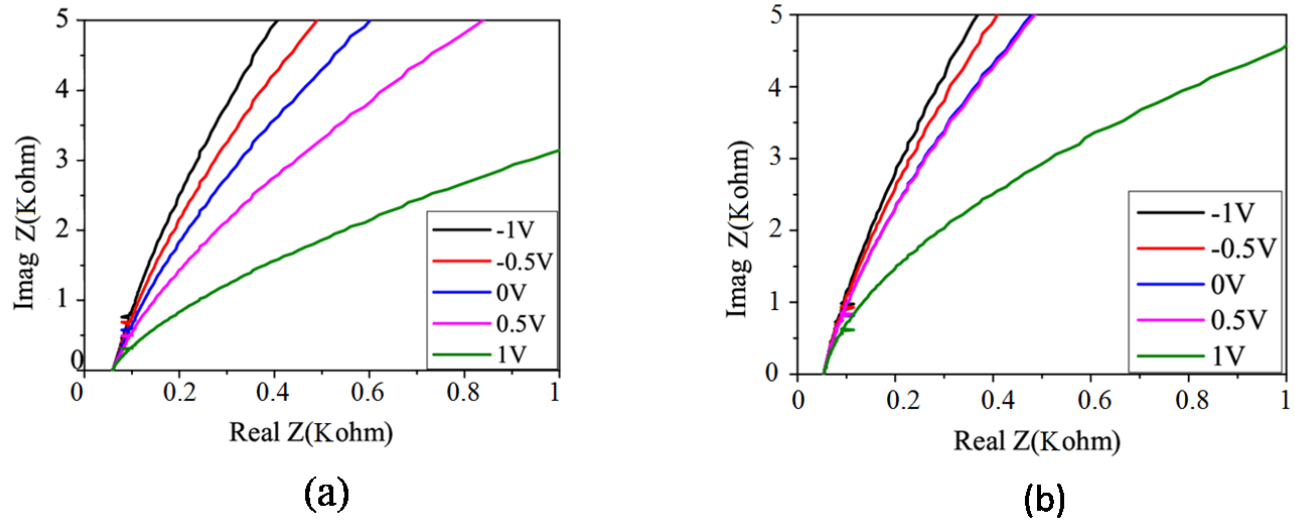

Fig. 12. Cole-Cole plot (a) Device A(2000 rpm)(b) Device C(4000 rpm) (color online)

The Nyquist curves of ITO/PTAA/P3HT:PCBM/Al measured at different bias voltages with the Devices A and C are shown in Fig. 12(a) and 12(b). In the plot, it can be seen that the size of the semicircle, which indicates higher R_p is higher for device C. The resistance R_p, in the equivalent circuit, corresponds to the charge transport through the device and this means [29] that the charge transfer is faster in device A.

4. Conclusion

The effect of PTAA as a hole transport layer for the bulk heterojunction OPV devices are investigated in terms of different layer thicknesses formed by the spinning speeds of 2000 rpm, 3000 rpm and 4000 rpm. The device current-voltage characteristics were obtained under both dark and illumination. devices were determined from the dark characteristics. The reverse saturation current is found to reduce and barrier potential increases for devices with active layer formed at higher spinning speeds. The rectification ratio was found to be highest for device A formed at the lowest spinning speed for which the carrier mobility and the power conversion efficiency are greater. Thouh the efficency of the deices are found to be very low, the investigations helped to provide valuable indsight on the effect of hydrophobicity of the PTAA layer on the morphology of the BHJ layer. The mobility and other parameters extracted using impedence spectroscopy also helped to evlaluate the potential use of PTAA as hole transport layer in P3HT-PCBM based organic solar cells.

Acknowledgements

The financial support provided from TEQIP-II Project, TKM College of Engineering, Kollam-5, Kerala,

India is gratefully acknowledged. The authors also thank and acknowledge the ANERT, Kerala, for the financial support. All the support given by the Sree Ayyappa College, Chengannur, Kerala, India is also thankfully acknowledged.

References

[1] M. Erray, M. Hanine, E. Boufounas, A. El Amrani, Eur. Phys. J. Appl. Phys. **82**, 30201 (2018).
[2] Z. Yin, J. Wei, Q. Zheng, Adv. Sci. **3**(8), 1 (2016).
[3] S. Cong, X. Llu, Y. Jiang, W. Zhang, Z. Zhao, The Innovation **1**, 100051 (2020).
[4] M. Liu, Y. Shi, M. Wu, Y. Tian, H. Wei, Q. Sun, M. Shafi, B. Man, J. Raman Spectrosc. **51**(5), 750 (2020).
[5] Y. Li, L. Yu, L. Chen, C. Han, H. Jiang, Z. Liu, N. Zheng, J. Wang, M. Sun, R. Yang, X. Bao, The Innovation **2**, 100090 (2021).
[6] H. Jiang, X. Li, H. Wang, Z. Ren, N. Zheng, X. Wang, Y. Li, W. Chen, R. Yang, Adv. Sci. **7**(7), 1903455 (2020).
[7] K. Miandal, K. A. Mohamad, A. Alias, J. Adv. Res. in Mat. Sci. **1**(1), 7 (2016).
[8] S. Yoon, H. Kim, E. Shin, Y. Noh, B. Park, I. Hwang, Phys. Status Solidi A **213**(9), 2431 (2016).
[9] Y. Kim, E. H. Jung, G. Kim, D. Kim, B. J. Kim, J. Seo, Adv. Energy Mater. **8**(29), 1801668 (2018).
[10] P. P. Khlyabich, B. Burkhart, A. E. Rudenko, B. C. Thompson, Polymer **54**(20), 5267 (2013).
[11] G. Ligorio, N. Z. Morales, E. J. W. List-Kratochvil, Appl. Phys. Lett. **116**(24), 241603 (2020).
[12] K. L. Usha Kumary, M. Pratheek, T. A Shahul Hameed, P. Predeep, AIP Conf. Proc. **2162**, 020137 (2019).
[13] K. L. Usha Kumary, M. Pratheek, T. A. Shahul Hameed, P. Predeep, AIP Conf. Proc. **2222**, 020016 (2020).
[14] S. M. Sze, K. K. Ng, "Physics of Semiconductor Devices", 3rd Edn., John Wiley and Sons, New Jersey 141, 2007.
[15] Z. Ul Islam, M. Tahir, W. A. Syed, F. Aziz, F. Wahab, S. M. Said, M. R. Sarker, S. H. Md Ali, M. F. M. Sabri, Energies **13**(4), 962 (2020).
[16] Ö. T. Özmen, Microelectron. Reliab. **54**(12), 2766 (2014).
[17] M. M. Makhlouf, M. M. El-Nahas, M. H. Zeyada, Mater. Sci. Semicond. Process. **58**, 68 (2017).
[18] H. G. B. Olyaee, P. J. S. Foot, V. Montgomery, J. Theor. Appl. Phys. **9**(4), 315 (2015).
[19] H. Li, D. He, Q. Zhou, P. Mao, J. Cao, L. Ding, J. Wang, Sci. Rep. **7**, 40134 (2017).
[20] J. Mullerova, M. Kaiser, V. Nadazdy, P. Siffalovic, E. Majkova, J. Sol. Energy **134**, 294 (2016).
[21] X. Liu, L. J. Guo, Y. Zheng, Nanoscale Res. Lett. **12**, 1 (2017).
[22] H. Yu, Y. Li, Y. Dong, X. Huang, Int. J. Photoenergy **2016**, 1 (2016).
[23] B. Lim, J. Jo, S. Na, J. Kim, S. Kim, D. Kim, J. Mater. Chem. **20**(48), 10919 (2010).
[24] M. Neukom, S. Zufle, S. Jenatsch, B. Ruhstaller, Sci. Technol. Adv. Mater. **19**(1), 291 (2018).
[25] M. Benhaliliba, T. Asar, S. Ozcelik, Optik **217**, 164791 (2020).
[26] O. Almora, C. Aranda, E. Mas-Marza, G. Garcia-Belmonte, Appl. Phys. Lett. **109**, 173903 (2016).
[27] C. Wang, Z. Zhang, S. Pejic, R. Li, M. Fukuto, L. Zhu, G. Sauve, Macromolecules **51**(22), 9368 (2018).
[28] Z. Li, W. Guo, C. Liu, X. Zhang, S. Li, J. Guo, L. Zhang, Phys. Chem. Chem. Phys. **19**(31), 20839 (2017).
[29] C. A. Otalora, A. F. Loaiza, G. Gordillo, Adv. Mater. Sci. Eng. **2016**, 1 (2016).

*Corresponding author: predeep@nitc.ac.in